Journal of
Ceramic Science
and Technology

J. Ceram. Sci. Tech., **06** [02] 105-112 (2015)
DOI: 10.4416/JCST2014-00057
available online at: http://www.ceramic-science.com

Porous Geopolymer Components through Inverse Replica of 3D Printed Sacrificial Templates

G. Franchin*[1], P. Colombo[1, 2]

[1]Department of Industrial Engineering, University of Padova, Via Marzolo 9, 35131 Padova, Italy
[2]Department of Materials Science and Engineering, The Pennsylvania State University, University Park, PA 16801, USA

received December 29, 2014; received in revised form February 2, 2015; accepted February 26, 2015

Abstract

Geopolymeric components with high controlled porosity were designed and produced by means of CAD/CAM and FDM (Fused Deposition Modeling) techniques. PLA sacrificial structures with different patterns were 3D printed with high accuracy and a geopolymeric slurry was used to produce close inverse replicas by means of impregnation in vacuum conditions and subsequent geopolymerization reaction and template removal in a combined chemical and thermal treatment. The FDM-manufactured sacrificial structures replicated the computationally designed porosity to be obtained in the final geopolymer components in terms of total porosity, average pore size and pore architecture. Geopolymer features were not affected by the fabrication route, and the process resulted in highly porous geopolymeric components with well-defined interconnected channels designed at both the macro- and microscopic scale. The specific surface area of the samples was ~ 23 m^2/g. The total porosity of the samples ranged from ~ 66 to ~ 71 vol%, given both by the designed geometrical macroporosity and by the inherent chemical micro- and meso-porosity of the geopolymer.

Keywords: Geopolymers, solid freeform fabrication, fused deposition modeling, inverse replica, 3D printing

I. Introduction

Solid freeform fabrication (SFF) technologies enable the fabrication of 3D structures based on a layer-by-layer approach starting from numerical models. After the development of stereolithography in the 1980s [1], numerous competing SFF technologies have been introduced and improved with the focus moving from rapid prototyping to production of finished and functional devices. Additive Manufacturing (AM) systems based on SFF technology have the peerless ability to produce designs impossible to build otherwise; this is particularly relevant in sectors such as tissue engineering [2], specialized mechanical components [3] and art design. Most initial AM systems were based mainly on the use of various polymers, but nowadays metal powder or metal-filament-based systems have been successfully developed and have become a big business, driven especially by the aerospace industry [4–7]. The direct 3D printing approach with ceramics faces unique challenges and has several drawbacks: it requires custom machines, extensive operator expertise and, this is the main challenge, careful optimization of the material's rheological properties to find slurry compositions, including binders, which could be viably used with the few existing 3D printing machines [8–11].

An indirect, inverse replica approach where (macro-)porous structures (molds) are printed and the ceramic slurry is cast into the mold cavity can overcome some of the limitations of the direct printing technique. In this way, molds can be produced with high accuracy with common polymers, taking advantage of freedom and shape possibilities provided by this technique with little effort. Moreover, limitations in terms of the homogeneity and microstructure control of the final ceramic part can be overcome by filling the templates with a suitable slurry. Finally, the requirements in terms of rheological behavior for the infiltrating slurries are much less stringent in comparison to the strict control required for the fabrication of high-quality structures by direct printing. In 1998, Bose *et al.* [12] fabricated 3D honeycomb porous alumina structures for bone implants by infiltrating a polymeric mold created by means of stereolithography with a ceramic slurry. SFF methods can be used to create scaffolds with channels possessing non-random connectivity designed to create a porous network at a macroscopic scale across the structure; these methods provide excellent control over the external shape and the internal interconnectivity and geometry, but micro-scale resolution is usually poor.

Little experimentation has been carried on in the last years in the field of porous components produced by inverse replica, and almost exclusively for tissue engineering applications. Preliminary attempts involved manual building of predesigned macroporous architectures where sugar porogen elements were stacked layer-by-layer to form uniaxial, orthogonal and helicoidal networks

* Corresponding author: giorgia.franchin@dii.unipd.it

in polymeric structures [13]. A few years later, PLA scaffolds and PLA-hydroxyapatite scaffolds were fabricated by casting in 3D-printed wax/PSA molds. The same route was followed by Ma in 2004 [14] providing highly accurate inverse replicas with promising features for tissue engineering applications.

In terms of more complex sacrificial templates, by means of computer tomography molds can be designed to replicate, for instance, the shape of a bone defect or a zygoma [15]. The interest of the field lies now in the combination of intricate architectures at a scale spanning three orders of magnitude: macro (external shapes), micro (pores) and nano (fibers), as demonstrated for instance, by Chen *et al.* [16] with PLLA nano-fibrous scaffolds. Local pores can be manufactured simultaneously with the infiltration process using conventional methods (e.g. using emulsions or adding sacrificial particles to the infiltrating slurry), producing both local and global pores within one sample. In this work we combined, for the first time, an inverse SFF fabrication technique with geopolymers, a novel class of materials that possesses a high degree of intrinsic micro (< 2 nm) and meso-porosity (2 – 50 nm).

Geopolymers are inorganic materials with a chemical composition similar to that of zeolite and a variable microstructure (amorphous to semi-crystalline). They are synthesized from a reaction that occurs between SiO_2 and Al_2O_3 species in a highly alkaline medium, leading to the formation of a continuous three-dimensional inorganic network. These materials can consolidate at low, even room temperature, enabling the retention of the produced shape and offering the possibility of efficiently producing highly porous ceramic components suitable for filtering applications [17].

II. Materials and Methods

Sacrificial templates were designed and converted into stereolithography (STL) data using an open source CAD/CAM software (FreeCAD); the model was then imported into a software (Repetier, Hot-World GmbH & Co. KG, Germany) that sliced it into layers and converted to a .gcode path for direct 3D printing using a PowerWASP EVO (WASP, Italy) Fused Deposition Modeling (FDM) 3D printer. A FDM printer works by laying down material in layers; a thermoplastic filament is unwound from a coil and supplies material to produce a part by extruding small portions of material to form layers. The extrusion nozzle is heated to melt the material, the flow can be turned on and off and there is typically a worm-drive that pushes the filament into the nozzle at a controlled rate. The material hardens immediately after extrusion, thereby allowing the correct object shape to be maintained. A Poly(Lactic Acid) (PLA) filament (3 mm diameter; WASP, Italy) was used to print the molds with a resolution of 100 μm in the Z direction (which determines the height of each layer) and of 350 μm in the X, Y directions, corresponding to the nozzle diameter.

The external shape of the final lattice was a cube with 15-mm sides; molds were designed to have open interconnected channels of (W x H) 3 x 3 mm or 1.5 x 3 mm. The molds had three sides closed with the sacrificial material as to avoid leaking of the slurry during infiltration, and a lip was also designed in order to hold the excess slurry during infiltration. Four different channel designs were tested.

Sacrificial templates were impregnated with a geopolymer slurry; Argical-M 1200S, an artificial metakaolin ($Al_2Si_2O_7$) obtained by micronizing and calcining a kaolinitic clay ($Al_2Si_2O_5(OH)_4$) from the Charentes basin (Imerys Refractory Minerals (France)), and fly ash class F (200 mesh; Tractebel Energia (Brazil)) were used as geopolymeric precursors; their composition is reported in Table 1. Potassium hydroxide (KOH) pellets (85 % purity, Dinâmica Química Contemporânea Ltda (Brazil)) and potassium silicate solution (Si/K = 2 – 2.1, density 1.32 – 1.34 g/cm^3, viscosity 100 – 300 mP; KSIL 0465, Crosfield Italia Srl) were used as alkaline activators.

Table 1: Composition of the Argical M1200S and fly ash raw materials (wt%).

	Argical M1200S	Fly ash
SiO_2	55	55.3
Al_2O_3	39	19.8
Fe_2O_3	1.8	10.2
Na_2O	1	0
K_2O		2.3
TiO_2	1.5	1
CaO	0.6	1.3
MgO		0.7

The first step in the preparation of the geopolymer slurry was the preparation of a 15M KOH solution. Once KOH had dissolved completely in distilled water, a solution of potassium-based activators (potassium hydroxide and potassium silicate) was prepared in a mixer (500 rpm, 5 min, Ika-Werke Ost Basic, Staufen, Germany), according to the following weight ratio: 1.86 silicate solution : 1 KOH 15M. The activating solution was prepared 24 hours in advance to let the silicate dissolve completely in the basic solution [16]. Metakaolin was added at room temperature and stirred at 800 rpm for 30 min, followed by the addition of the fly ash and stirring at 1000 rpm for other 30 min. An addition of 50 wt% fly ash in respect of metakaolin was used. Based on these raw materials, the geopolymer slurry resulted in the following oxide molar ratios: $SiO_2/Al_2O_3 = 4$, $K_2O/SiO_2 = 0.25$ and $H_2O/K_2O = 15.83$.

As soon as the slurry was homogeneous, the infiltration process was performed; the slurry was poured into the molds and then put under rotary-pump-vacuum (~ 0.1 Pa) for 15 min. After that, molds were sealed with cling film and left at room temperature for 48 – 72 h to allow for the completion of the geopolymerization reaction.

After the reaction was completed, the sacrificial PLA templates had to be removed; samples were first directly immersed in KOH 15M at a temperature of 72 °C for 24 h; with the help of the temperature, the basic solution carried out a nucleophilic attack of the polymer chain

links, leading to their partial hydrolysis and condensation [18]. Samples were then washed with hot water to extract the PLA; this step can also be used to confirm the extent of the geopolymerization reaction, since non-fully-condensed geopolymer materials are sensitive to water and undergo swelling or complete destruction [19]. Subsequently, the samples were heat-treated at 330 °C for 24 h in a tube furnace (Carbolite CWF1200, Derbyshire, UK) under an air flux (heating rate 1 °C). This coupled chemo-thermal treatment had been already tested by Okada *et al.* [20], giving good results in terms of complete PLA removal and retention of the geopolymer integrity.

The morphology and microstructure of the samples were investigated using an optical stereoscope (Wild Heerbrugg, Type 376788, coupled with a digital camera) and an Environmental Scanning Electron Microscope (FEI Quanta200 ESEM, Eindhoven, The Netherlands). X-ray diffraction analysis (XRD, Bruker AXS-D8 advance, Karlsruhe, Germany) was performed on powdered samples using $CuK_{\alpha 1}$ radiation (10 – 70° 2θ, 2 s/step). Semi-automatic crystalline phase identification was performed using the Match! software package (Crystal Impact GbR, Bonn, Germany), supported by data from PDF-2 database (ICDD-International Center for Diffraction Data, Newtown Square, PA, USA). The true density (skeleton density) of the geopolymer material was measured with a helium pycnometer on finely crushed powders (Accupyc 1330, Micromeritics, Norcross, GA). Since the macropores derived from the CAD/CAM designs are too large to entrap liquid, it was not possible to measure the amount of macro-porosity using the Archimedes' approach. The open, closed and total porosity of the struts was quantified by the Archimedes' method using water as the infiltrating fluid. The amount of total porosity of the entire lattices was evaluated based on geometrical considerations on the models and the measurement of their weight on a precision digital scale (divided by the lattices' volume). Specific surface area (SSA) data were collected in N_2 adsorption experiments at liquid nitrogen temperature using a Quantachrome Nova Station A (Quantachrome Instruments, Boynton Beach, USA). All the samples were degassed at 250 °C prior to the nitrogen adsorption measurements. The Brunauer-Emmett-Teller specific surface area (SSA) was determined with the multipoint BET method using the adsorption data in the relative pressure (P/P_0) range of 0.05 – 0.3.

III. Results and Discussion

Fig. 1 shows the different template designs used for the geopolymer impregnation (left) as well as the inverse lattices (right). The FDM-manufactured molds replicated the computationally designed desired macro-scale pore size and architecture; the solid struts in the PLA scaffold will constitute the macropores in the inverse replica structure. We selected these different structures because they would afford different characteristics to the final component in terms of different pressure drop, different mechanical properties, different contact time with the micro-/meso-porous solid struts, and possibly different thermal transport and fluid dynamic behavior with respect to the filtration medium.

The final lattices obtained after impregnation of the molds with the four different architectures, followed by the template removal, are shown in Fig. 2. We can observe that the geopolymeric lattices produced in this work were an accurate inverse replica of the 3D-printed structures; thanks to the complete and homogeneous infiltration under vacuum, the geopolymeric slurry was able to penetrate in all macroscopic cavities designed in the CAD/CAM projects. No shrinkage was observed after the geopolymerization of the slurry and no evidence of swelling was present, indicating that the geopolymerization reaction had proceeded to completion.

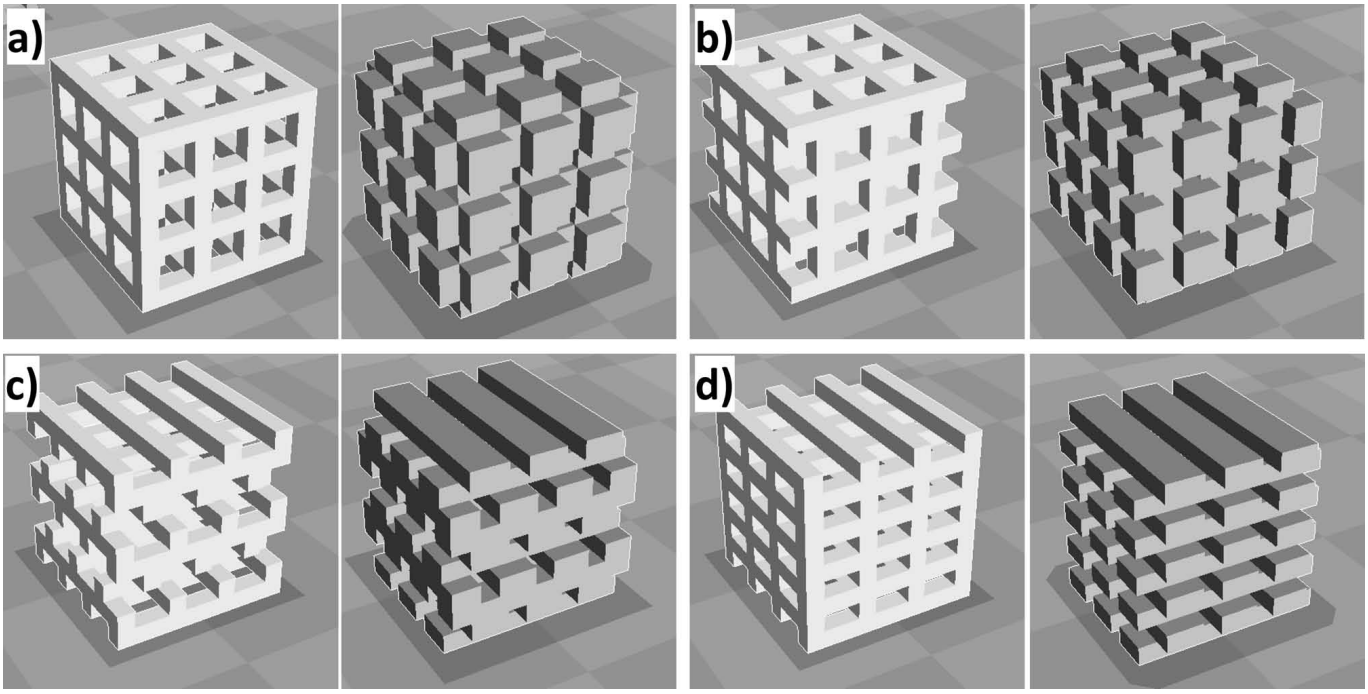

Fig. 1: 3D rendering of the sacrificial templates. Templates used for the geopolymer impregnation (left) and inverse lattices (right).

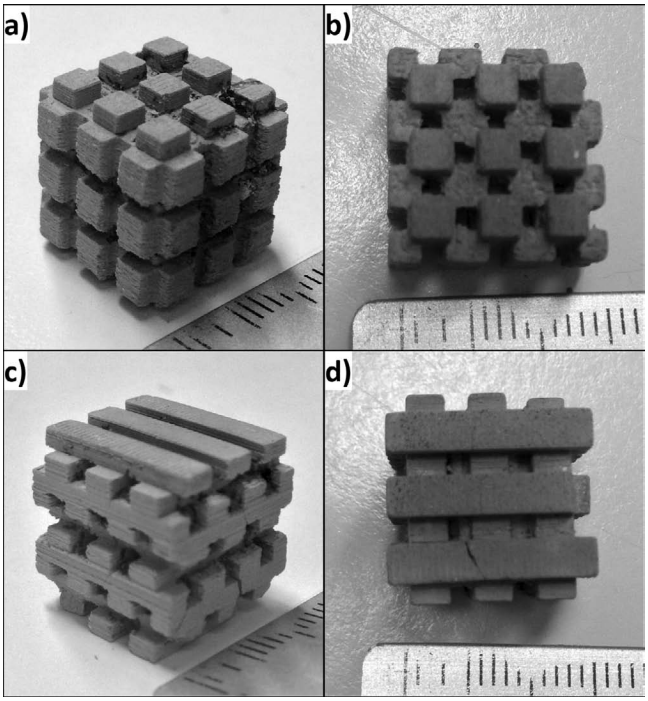

Fig. 2: Inverse replica of the four lattices after complete PLA degradation.

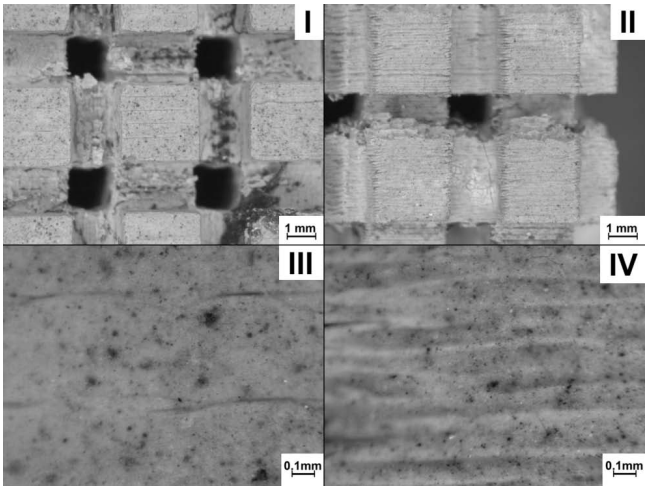

Fig. 3: Stereomicroscopic images of a lattice: (a) (I) top view; (II) side view; detail of top (III) and (IV) side surfaces showing their morphological characteristics (template-derived roughness).

Focusing the attention on one of the lattices, the one in Fig. 2a, we report in Fig. 3 the stereomicroscopic images at a higher magnification showing the top and side of the structure in detail. They show the regularity of the macropore structure and the lack of cracks or macroporosity embedded in the geopolymer matrix, and enable appreciation of the details of the morphology of the sample surface and of the strut material after PLA removal, in particular the template-derived roughness. In fact, the parallel grooves, observable in Fig. 3, are characteristic of the FDM process and are due to the layer-by-layer fused deposition of the molten PLA wire. They appear to have been very accurately replicated by the infiltrated geopolymeric matrix. We should also note that the way that the structures were built by FDM was different depending on the type of lattice produced. In order to generate the structures shown in Fig. 2c and 2d, the printing head deposited long PLA threads along the entire structure while, when printing the templates of Fig. 2a and 2b, PLA was deposited in much smaller areas, as only square columns with a 3 mm side size needed to be built. Laying out PLA in small areas, by FDM, allows less precision than that achievable when long filaments are deposited layer-by-layer. The structures, built with different accuracies, were closely replicated by the geopolymer matrix, indicating that the proposed templating approach based on the fabrication of highly interconnected sacrificial lattices by FDM is suitable for the fabrication of complex macroporous ceramic parts.

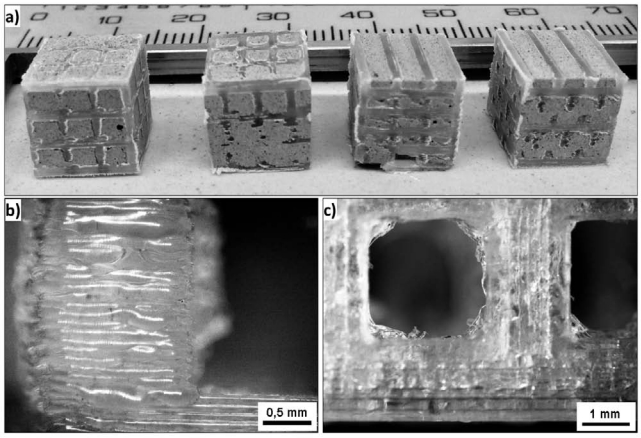

Fig. 4: Picture of some PLA templates infiltrated with the geopolymer slurry (a), and stereomicroscope details of the PLA template ((b): side view; (c): top view).

The PLA removal process combined a chemical and a thermal treatment. A simple direct thermal treatment of the impregnated samples resulted, in fact, in components containing several macroscopic cracks or sample destruction, because of the development of high thermal stresses upon heating caused by the large mismatch in the coefficient of thermal expansion between the geopolymer matrix and the polymeric scaffold. On the other side, the chemical treatment alone was found to be insufficient for a complete decomposition of the sacrificial polymeric template; therefore a combination of the two treatments had to be applied. In a few samples, occasional cracks could still be observed (see for instance Fig. 2d), suggesting the need to further improve the removal step of the PLA template, for instance by adjusting the heating rate. In Fig. 4 we show a picture of some PLA templates infiltrated with the geopolymer slurry (Fig. 4a) as well as stereomicroscope images of details of the PLA template (of the structure shown in Fig. 1a), showing the different resolution (surface smoothness) that was achieved depending on the printing direction (Fig. 4b: side view, resolution along the z axis; Fig. 4c: top view, resolution along x and y axes). In Fig. 4b the layer thickness was 100 μm, while in Fig. 4c the layer thickness was coincident with the wire dimension and was about 350 μm. In any case, the quality of the print is proven by the resolution and quality of the resulting geopolymeric structures. This suggests that it would be possible to employ strategies for modifying the surface morphology of the polymeric template, for instance, for further increasing the geometric surface area of the geopolymeric component and tailor the solid-fluid interaction in filtration or catalytic applications. In addition,

one could also just as easily infiltrate a geopolymer slurry in which either sacrificial particles or oil droplets are contained, in order to provide another level of complexity to the pore architecture of the component. As an example, in Fig. 5 we show stereomicroscope images of a sample (with an architecture obtained by infiltration of the structure shown in Fig. 1a), in which the slurry contained oil and hydrogen peroxide, resulting in foamed struts with partially interconnecting pores with a size ranging from ~ 50 to ~ 300 μm.

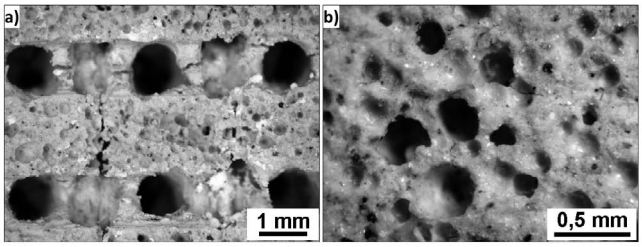

Fig. 5: Image of a sample (with an architecture obtained by infiltration of the structure shown in Fig. 1a), in which the slurry contained oil and hydrogen peroxide. a) general view; b) detail at higher magnification.

A more detailed view of the surface of the geopolymer matrix was provided with SEM investigations, see Fig. 6. Residual fly ashes (particularly rich in Fe and Ti) embedded in an amorphous/microcrystalline alumino-silicate matrix (gray areas) can be observed, as well as several small pores (black areas) with a size ranging from ~ 1 to ~ 10 μm, probably due to the evaporation of the excess water (the possibility that these pores were related to some residual air that was left embedded in the infiltrating slurry is rather remote, considering the fact that rotary vacuum was pulled on the system for several minutes during the infiltration).

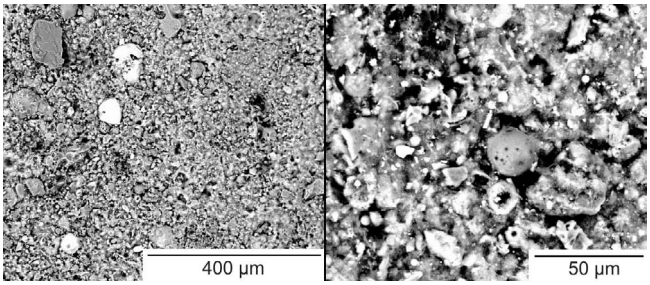

Fig. 6: SEM images of the surface of a geopolymer strut.

Scaffolds were crushed and the powders investigated by means of XRD analysis, which showed (Fig. 7) that the geopolymer matrix was mainly amorphous with some quartz and muscovite ($KAl_2(Si_3Al)O_{10}(OH,F)_2$) crystalline phases which are impurities in the metakaolin and typical for geopolymers not heat treated at high temperature [21].

Archimedes' measurements indicated that the geopolymer struts had a bulk density of 1.30 ± 0.01 g/cm^3 and an apparent one of 2.23 ± 0.01 g/cm^3, while pycnometer measurements gave a true density for the geopolymer material of 2.4367 ± 0.0002 g/cm^3. From these data, it was possible to calculate the porosity of the struts (see Table 2), while the determination of the bulk density of the lattices by weight and volume measurements allowed the total porosity of the structures to be obtained, which ranged from ~ 66 % to ~ 71 %. Note that the designed porosity was different among the various geopolymer scaffolds, and equal to 35.2 %, 40 %, 40 % and 36 vol% for structure a), b), c) and d) (see Fig. 1), respectively. Based on the porosity of the struts and on the volume of designed porosity, we also computed the total porosity; the data are in agreement with the measured total volume of porosity, and indicate that the absolute contribution of the struts' porosity to the total porosity was ~ 30 vol%. The difference between the amount of total measured and designed macroporosity can be due to partial damage to the edges of some struts in the produced structures as a result of handling or to imprecise measurements of the geometric dimensions of the samples.

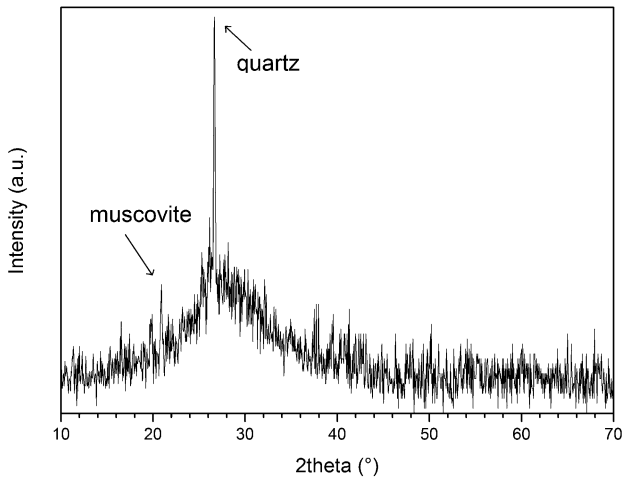

Fig. 7: XRD analysis of a sample of architecture (a) (see Fig. 1) after thermal treatment at 330 °C.

Table 2: Porosity of lattices and struts.

Lattice structure	a	b	c	d
Measured Lattice Total Porosity (vol%)	66.2 ± 1.0	70.9 ± 3.1	66.4 ± 0.8	70.2 ± 2.2
Computed Lattice Total Porosity (vol%)	65.5	68	65.9	68
Designed Lattice Macroporosity (vol%)	35.2	40	36	40
Struts Total Porosity (vol%)	46.72 ± 0.42			
Struts Open Porosity (vol%)	41.87 ± 0.67			
Struts Closed Porosity (vol%)	4.85 ± 0.55			

While the macroscopic open channels, with a designed size and volume, enable suitable permeability for liquid or gas through the porous scaffold, the solid struts are responsible for the interaction with the fluid when the component is used for filtration or as a catalytic support. They contain up to ~ 40 vol% of open and interconnected porosity (see Table 2), and their inherent chemical micro- and meso-porosity is due to the polycondensation of alumino-silicates during geopolymerization reaction, which produces water, and the fact that their morphology at the nanometric scale is based on the assemblage of small spheroidal particles [22]. The N_2 adsorption and desorption curves are reported in Fig. 8; the isotherms can be classified as type IV, according to the International Union of Pure and Applied Chemistry (IUPAC), proving that both micropores (diameter < 2 nm, detected by N_2 adsorption at $P/P_0 < 0.15$) and mesopores (diameter = 2 – 50 nm, detected by the hysteresis at higher values of relative pressure) are present. The specific surface area of the samples was 22.991 m^2/g, which is similar to values reported in literature for potassium-containing geopolymers based on metakaolin and fly ash [23 – 28]. As this is inherent porosity that develops in the system because of the geopolymerization reaction, it was not affected by the application of vacuum for several minutes during infiltration of the slurry.

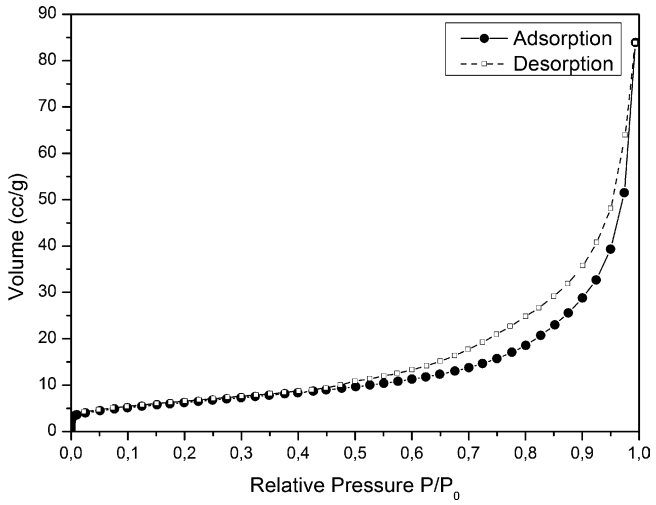

Fig. 8: Adsorption and desorption isotherms on powders obtained by crushing a geopolymer scaffold of architecture (a) (see Fig. 1).

Thanks to an accurate design of both the template shape and the geopolymer material, we were able to reach in the final components a suitably large amount of total porosity, mostly composed of open porosity, which is of course the predominant feature needed in filters.

Preliminary mechanical strength data gave an average compressive strength value of ~ 8.5 MPa for a sample with an architecture (a) (see Fig. 1), indicating that the components could indeed be suitable for use in filtering applications.

Future work will include the incorporation of more interconnected porosity in the solid struts, increasing the specific surface area by means of chemical additives (e.g. oil), and characterization of the mechanical and permeability properties of the different lattices.

IV. Conclusions

Geopolymer components with controlled porosity were designed and produced by means of CAD/CAM and FDM techniques. PLA sacrificial templates with different patterns were 3D printed with high accuracy, and a geopolymer slurry was used to produce close inverse replicas by impregnation in vacuum conditions and subsequent geopolymerization reaction and template removal by a combined chemical and thermal treatment. The advantage of this process over direct 3D printing is that no careful optimization of the rheology of ceramic slurry is necessary, and some of the drawbacks of direct 3D printing, such as microstructural inhomogeneity, can be avoided. Geopolymer features were not affected by the processing, and the samples possessed highly interconnected macroscopic channels and micro- and meso-porosity in the struts, making them potentially attractive for filtering or catalyst support applications.

Acknowledgements

The authors would like to gratefully acknowledge Imerys Refractory Minerals (France) for kindly providing the Argical-M 1200S metakaolin. GF is grateful for the useful discussions and assistance provided by Marcelo Strozi Cilla of Universidade Federal de São Carlos, Brazil.

References

1 Hull, W.C.: Apparatus for production of three-dimensional objects by stereolithography, US 06/638,905, (1984).

2 Yang, S., Leong, K., Du, Z., Chua, C.: The design of scaffolds for use in tissue engineering. Part II: Rapid prototyping techniques, *Tissue Eng.*, **8**, [1], 1 – 11, (2002).

3 Bertsch, A., Bernhard, P., Vogt, C., Renaud, P.: Rapid prototyping of small size objects, *Rapid Prototyping J.*, **6**, 259 – 266, (2000).

4 Abe, F., Osakada, K., Shiomi, M., Uematsu, K., Matsumoto, M.: The manufacturing of hard tools from metallic powders by selective laser melting, *J. Mater. Process. Tech.*, **111**, 210 – 213, (2001).

5 Agarwala, M., Bourell, D., Beaman, J., Marcus, H., Barlow, J.: Direct selective laser sintering of metals, *Rapid Prototyping J.*, **1**, 26 – 36, (1995).

6 Atzeni, E., Salmi, A.: Economics of additive manufacturing for end-usable metal parts, *Int. J. Adv. Manuf. Tech.*, **62**, 1147 – 1155, (2012).

7 Brandl, E., Baufeld, B., Leyens, C., Gault, R.: Additive manufactured Ti-6Al-4V using welding wire: comparison of laser and arc beam deposition and evaluation with respect to aerospace material specifications, *Physics Procedia*, **5**, Part B, 595 – 606, (2010).

8 Lewis, J.A.: Direct-write assembly of ceramics from colloidal inks, *Curr. Opin. Solid St. M.*, **6**, 245 – 250, (2002).

9 Travitzky, N., Bonet, A., Dermeik, B., Fey, T., Filbert-Demut, I., Schlier, L., Schlordt, T., Greil, P.: Additive manufacturing of ceramic-based materials, *Adv. Eng. Mater.*, **16**, 729 – 754, (2014).

10 Schlordt, T., Schwanke, S., Keppner, F., Fey, T., Travitzky, N., Greil, P.: Robocasting of alumina hollow filament lattice structures, *J. Eur. Ceram. Soc.*, **33**, 3243 – 3248, (2013).

11 Mühler, T., Gomes, C.M., Heinrich, J., Günster, J.: Slurry-based additive manufacturing of ceramics, *Int. J. Appl. Ceram. Tec.*, **12**, 18 – 25, (2015).

12 Bose, S., Avila, M., Bandyopadhyay, A.: Processing of bioceramic implants via fused deposition process. In: '98 SFF. Austin, TX., 1998.

13 Zhang, R., Ma, P.X.: Synthetic nano-fibrillar extracellular matrices with predesigned macroporous architectures, *J. Biomed. Mater. Res.*, **52**, 430 – 438, (2000).

14 Ma, P.X.: Scaffolds for tissue fabrication, *Mater. Today*, **7**, 30 – 40, (2004).

15 Lee, M., Dunn, J.C.Y., Wu, B.M.: Scaffold fabrication by indirect three-dimensional printing, *Biomaterials*, **26**, 4281 – 4289, (2005).

16 Chen, V.J., Smith, L.A., Ma, P.X.: Bone regeneration on computer-designed nano-fibrous scaffolds, *Biomaterials*, **27**, 3973 – 3979, (2006).

17 Strozi Cilla, M., Morelli, M.R., Colombo, P.: Open cell geopolymer foams by a novel saponification/peroxide/gelcasting combined route, *J. Eur. Ceram. Soc.*, **34**, 3133 – 3137, (2014).

18 Coszach, P., Bogaert, J., Willocq, J.: Chemical recycling of PLA by hydrolysis, PCT/EP2010/054274, (2010).

19 Davidovits, J.: Geopolymers, *J. Therm. Anal. Calorim.*, **37**, 1633 – 1656, (1991).

20 Okada, K., Imase, A., Isobe, T., Nakajima, A.: Capillary rise properties of porous geopolymers prepared by an extrusion method using polylactic acid (PLA) fibers as the pore formers, *J. Eur. Ceram. Soc.*, **31**, 461 – 467, (2011).

21 Bignozzi, M.C., Manzi, S., Lancellotti, I., Kamseu, E., Barbieri, L., Leonelli, C.: Mix-design and characterization of alkali activated materials based on metakaolin and ladle slag, *Appl. Clay. Sci.*, **73**, 78 – 85, (2013).

22 Davidovits, J.: Geopolymer chemistry and applications. 3rd edition. Institute Géopolymère, Saint-Quentin, 2011.

23 Bell, J.L., Driemeyer, P.E., Kriven, W.M.: Formation of ceramics from metakaolin-based geopolymers. Part II: K-based geopolymer, *J. Am. Ceram. Soc.*, **92**, 607 – 615, (2009).

24 Duxson, P., Lukey, G., van Deventer, J.J.: Physical evolution of Na-geopolymer derived from metakaolin up to 1000 °C, *J. Mater. Sci.*, **42**, 3044 – 3054, (2007).

25 Li, L., Wang, S., Zhu, Z.: Geopolymeric adsorbents from fly ash for dye removal from aqueous solution, *J. Colloid Interf. Sci.*, **300**, 52 – 59, (2006).

26 Cheng, T.W., Lee, M.L., Ko, M.S., Ueng, T.H., Yang, S.F.: The heavy metal adsorption characteristics on metakaolin-based geopolymer, *Appl. Clay. Sci.*, **56**, 90 – 96, (2012).

27 Medpelli, D., Seo, J., Seo, D.: Geopolymer with hierarchically Meso-/Macroporous structures from reactive emulsion templating, *J. Am. Ceram. Soc.*, **97**, 70 – 73, (2014).

28 Strozi Cilla, M., Raymundo Morelli, M., Colombo, P.: Effect of process parameters on the physical properties of porous geopolymers obtained by gelcasting, *Ceram. Int.*, **40**, 13585 – 13590, (2014).